

# Large Eddy Simulation of Turbulent Channel Flows by the Rational LES Model

T. Iliescu and P. Fischer

October 25, 2018

## Abstract

The rational large eddy simulation (RLES) model is applied to turbulent channel flows. This approximate deconvolution model is based on a rational (subdiagonal Padé) approximation of the Fourier transform of the Gaussian filter and is proposed as an alternative to the gradient (also known as the nonlinear or tensor-diffusivity) model. We used a spectral element code to perform large eddy simulations of incompressible channel flows at Reynolds numbers based on the friction velocity and the channel half-width  $Re_\tau = 180$  and  $Re_\tau = 395$ . We compared the RLES model with the gradient model. The RLES results showed a clear improvement over those corresponding to the gradient model, comparing well with the fine direct numerical simulation. For comparison, we also present results corresponding to a classical subgrid-scale eddy-viscosity model such as the standard Smagorinsky model.

# 1 Introduction

Large eddy simulation (LES) is one of the most successful techniques in the numerical simulation of turbulent flows. Contrary to the direct numerical simulation (DNS), which tries to capture all the scales in the flow, LES aims at resolving only the large-scale flow features. The large scales are defined by means of a filtering operation: the Navier-Stokes equations are convolved with a spatial filter, and the resulting filtered variables become the variables of interest in LES. Thus, a good LES model should be able to compute an accurate approximation of the filtered variables.

An essential challenge in LES is the modeling of the subgrid-scale (SGS) stresses, representing the interactions between the large (above the filter width) and small (below the filter width) scales in the filtered Navier-Stokes equations. A remarkable research effort has led to a wide variety of SGS models, surveyed, for example, in [1], [2], and [3].

Arguably the most popular class of LES models is the eddy-viscosity type, based on (variants of) the Smagorinsky model [4]. The main feature of the eddy-viscosity models is that they properly transfer kinetic energy (by inviscid processes) from large scales to smaller and smaller scales, until this energy is dissipated through viscous effects. These models have several limitations, however, including poor correlation coefficients in a priori tests [5], [6] and inability to provide backscatter. Some of these limitations are circumvented by using a dynamic procedure in calculating the Smagorinsky constant, yielding the dynamic subgrid-scale eddy-viscosity model introduced by Germano et al. [7], and used in many studies [8], [9].

Another class of SGS models is the scale-similarity one. The scale-similarity model, introduced by Bardina et al. [6], postulates that the full structure of the velocity field at scales below the filter width is similar to that at scales above the filter width. A priori tests [6] show high correlations between real and modeled stresses. Another realistic feature of the scale-similarity model is that it produces backscatter. In a posteriori tests, however, the scale-similarity model does not dissipate enough energy and typically leads to inaccurate results. As a remedy, Bardina et al. [6] added a dissipative Smagorinsky term. The resulting model, known as the mixed model, combines the strengths of both the scale-similarity and the Smagorinsky model. The dynamic procedure has been successfully applied to both the pure and the mixed scale-similarity model, yielding improved results [10].

A different class of SGS models consists of those models aimed at computing an improved SGS stress approximation by replacing the unknown unfiltered variables with approximately deconvolved filtered variables. An inverse filtered model was first proposed by Shah and Ferziger [11]. This idea was formalized by Geurts [12] for the top hat filter. Kuerten et al. [13] used the approximate inverse to improve the computable estimates in the dynamic Smagorinsky model. Another model in this class is the velocity estimation model of Domaradzki and Saiki [14], [15], [16]. Stolz and Adams [17] developed the approximate deconvolution model, based on repeated application of the filter to approximately deconvolve the

dependent variables [18], [19].

One popular model in this class is the gradient model (also known as the nonlinear or tensor-diffusivity model), which uses *explicit* filtering. In addition to the *implicit* filtering due to the effective truncations (grid and numerical method), this LES model also assumes a regular explicit filter of prescribed shape and effective width larger than the grid spacing.

The gradient model is based on a Taylor series approximation of the Fourier transform of the filter and aims at reconstructing the filtered-scale stress due to explicit filtering. The gradient model was developed in several steps. First, in 1974 Leonard [20] proposed a model for the “resolved scales”  $\overline{\mathbf{u}} \overline{\mathbf{u}}$  in the Reynolds stress tensor. Next, in 1979 Clark, Ferziger, and Reynolds [5] used the same approach to model the “cross-terms”  $\overline{\mathbf{u}\mathbf{u}'} + \overline{\mathbf{u}'\mathbf{u}}$ .

The gradient model was tested a priori against experimental data (two-dimensional cuts) by Liu et al. [21]. Borue and Orszag [22] presented a detailed a priori analysis of the gradient model based on Gaussian-filtered DNS of homogeneous, isotropic decaying turbulence. Also, Winckelmans et al. [23] presented several a priori tests for the gradient model and its dynamic version, again in the context of homogeneous, isotropic decaying turbulence. Similar tests have been performed by Carati et al. [24]. All the above a priori tests have shown high correlations.

In *a posteriori* tests, however, it was found that the gradient model does not dissipate enough energy. Simulations with the pure gradient model appear to be unstable [25]. Also, Liu, Meneveau, and Katz [21] reported problems near the wall, where the pure gradient model’s Reynolds stresses do not follow the  $x_2^3$  behavior. To stabilize the gradient model, Clark, Ferziger, and Reynolds [5] combined it with a Smagorinsky term, but the resulting mixed model inherited the excessive dissipation of the Smagorinsky model. A different approach was proposed by Liu et al. [21], who supplied the gradient model with a “limiter” to prevent energy backscatter; this clipping procedure ensures that the model dissipates energy from large to small scales. This approach was also used in [26], [27].

From this point of view, the gradient model is similar to the scale-similarity model: it shows high correlations in a priori tests, but it does not dissipate enough energy in actual LES simulations: hence the need for extra viscosity type terms (mixed models). We note that, for both types of model, the best results in actual LES simulations were obtained by using the dynamic mixed procedure [28], [23]. In fact, it has been noted before [28], [9], [24], [23] that there are strong ties between the gradient model and the scale-similarity model: the first term in the Taylor series expansion of the scale-similarity model is indeed the gradient model. As noted by Winckelmans et al. [23], however, the other terms in the expansion are different. Thus, the gradient model is not identical to the scale-similarity model.

The model presented in this paper was introduced by Galdi and Layton [29] as an alternative to the gradient model. They observed that the Taylor series approximation of the Fourier transform of the Gaussian filter used in the derivation of the gradient model actually *increases* the high wave number components, instead of damping them. As an alternative to the Taylor series approximation, Galdi and Layton proposed a rational ((0,1) Padé) approx-

imation. This rational approximation is consistent with the original approximated function (which is a negative exponential): it attenuates the high wave number components.

In this paper, the resulting LES model, called in the sequel the rational LES (RLES) model, is applied to the numerical simulations of incompressible channel flows at  $Re_\tau = 180$  and  $Re_\tau = 395$ .

## 2 The Rational LES Model

The usual LES starts by convolving the Navier-Stokes equations (NSEs) with a spatial filter  $g_\delta$ . Assuming that differentiation and convolution commute (which is true for homogeneous filters), the filtered NSEs read as follows:

$$\bar{\mathbf{u}}_t + \nabla \cdot (\overline{\mathbf{u}\mathbf{u}}) - Re^{-1} \Delta \bar{\mathbf{u}} + \nabla \bar{p} = \bar{\mathbf{f}}, \quad (1)$$

where  $\delta$  is the filter width and  $\bar{\mathbf{u}} = g_\delta * \mathbf{u}$  is the variable of interest. The filtered NSEs (1) do not form a closed system, and a considerable research effort in LES research has been directed at modeling the stress

$$\tau = \overline{\mathbf{u}\mathbf{u}} - \bar{\mathbf{u}} \bar{\mathbf{u}}. \quad (2)$$

As mentioned by Carati et al. [24], this stress consists of a filtered-scale stress tensor, mainly due to filtering, and a subgrid-scale (SGS) stress tensor, mainly due to discretization. One way of approximating the filtered-scale stress tensor is by using a Taylor series expansion in the wave number space to represent the unknown full velocity in terms of the filtered velocity. This approach was first used by Leonard [20], and it was later espoused by Clark, Ferziger, and Reynolds [5]. The resulting model, called the gradient, nonlinear, or tensor-diffusivity model, was used in numerous studies [20], [5], [24], [22], [23], [30], [21], [31], [32].

The gradient model is derived by using a Taylor series approximation to the Fourier transform of the Gaussian filter

$$\widehat{g}_\delta(\mathbf{k}) = e^{-\frac{\delta^2 |\mathbf{k}|^2}{4\gamma}} \approx 1 - \frac{\delta^2 |\mathbf{k}|^2}{4\gamma} + O(\delta^4), \quad (3)$$

and for its inverse

$$\frac{1}{\widehat{g}_\delta(\mathbf{k})} = e^{\frac{\delta^2 |\mathbf{k}|^2}{4\gamma}} \approx 1 + \frac{\delta^2 |\mathbf{k}|^2}{4\gamma} + O(\delta^4). \quad (4)$$

Decomposing  $\mathbf{u}$  into its average and its turbulent fluctuations

$$\mathbf{u} = \bar{\mathbf{u}} + \mathbf{u}', \quad (5)$$

and taking first the average and then the Fourier transform of the above relation, we get

$$\widehat{\mathbf{u}}' = \left( \frac{1}{\widehat{g}_\delta} - 1 \right) \widehat{\mathbf{u}}, \quad (6)$$

and thus,

$$\widehat{\mathbf{u}} = \frac{1}{\widehat{g}_\delta} \widehat{\mathbf{u}}, \quad (7)$$

where  $\widehat{\mathbf{u}}$  denotes the Fourier transform of  $\mathbf{u}$ .

By taking the inverse Fourier transform and using (4), we get

$$\mathbf{u} \approx \bar{\mathbf{u}} + \frac{\delta^2}{4\gamma} \Delta \bar{\mathbf{u}}. \quad (8)$$

By plugging the above into (2), using (3) and the same technique as above, simplifying, and dropping out the terms of  $O(\delta^4)$ , we get the gradient model

$$\tau = \overline{\mathbf{u}\mathbf{u}} - \bar{\mathbf{u}} \bar{\mathbf{u}} \approx \frac{\delta^2}{2\gamma} \nabla \bar{\mathbf{u}} \nabla \bar{\mathbf{u}}, \quad (9)$$

where

$$(\nabla \bar{\mathbf{u}} \nabla \bar{\mathbf{u}})_{i,j} = \sum_{l=1}^d \frac{\partial \bar{u}_i}{\partial \mathbf{x}_l} \frac{\partial \bar{u}_j}{\partial \mathbf{x}_l}. \quad (10)$$

Noticing that the approximation by Taylor series of  $\widehat{g}_\delta$  actually *increases* the high wave number components (see Figure 1), Galdi and Layton [29] developed a new LES model based on a rational ((0,1) Padé) approximation of  $\widehat{g}_\delta$ , which preserves the decay of the high wave number components:

$$\widehat{g}_\delta(\mathbf{k}) = e^{-\frac{\delta^2 |\mathbf{k}|^2}{4\gamma}} \approx \frac{1}{1 + \frac{\delta^2 |\mathbf{k}|^2}{4\gamma}} + O(\delta^4). \quad (11)$$

The resulting LES model, called the rational LES (RLES) model, reads as follows:

$$\tau = \left[ \left( -\frac{\delta^2}{4\gamma} \Delta + I \right)^{-1} \left( \frac{\delta^2}{2\gamma} \nabla \bar{\mathbf{u}} \nabla \bar{\mathbf{u}} \right) \right]. \quad (12)$$

The inverse operator in (12) acts as a smoothing operator and represents the approximation of the convolution by the Gaussian filter in the stress tensor  $\tau$  in (2).

We note that differential filters have been proposed by Germano in [33]: Actually, one can think of (12) as the stress tensor obtained by applying such a differential filter. Mullen and Fischer used similar filters in [34]. Also, Domaradzki and Holm considered the Navier-Stokes-alpha model (which contains an inverse operator similar to the one in (12)), in an LES framework [35].

The mathematical analysis associated with the RLES model (12) was presented in [36]; the smoothing property of the inverse operator in (12) eliminated the necessity for using additional regularization operators (of eddy-viscosity type), as for the gradient model [37]. The first steps in the numerical analysis and validation of the RLES model (12) were made in [38] and [39], respectively.

This paper presents numerical results for the RLES model (12) applied to the 3D channel flow test problem at Reynolds numbers based on the wall shear velocity  $Re_\tau = 180$  and  $Re_\tau = 395$ . Some preliminary work started in [40]; it was significantly updated and improved in the present paper.

### 3 Numerical Setting

The 3D channel flow (Figure 2) is one of the most popular test problems for the investigation of wall bounded turbulent flows [41], [42]. We used the fine DNS of Moser, Kim, and Mansour [43] as benchmark for our LES simulations.

We compared the RLES model (12) with

- (I) the gradient model (9)  $\tau = \frac{\delta^2}{2\gamma} \nabla \bar{\mathbf{u}} \nabla \bar{\mathbf{u}}$ ;
- (II) the Smagorinsky model  $\tau = -(C_s \delta)^2 |\bar{S}| \bar{S}$ ;
- (III) a coarse DNS (no LES model),

where  $\bar{S} := \frac{1}{2}(\nabla \bar{\mathbf{u}} + \nabla \bar{\mathbf{u}}^T)$  is the deformation tensor of the filtered field,  $C_s = 0.1$  is the Smagorinsky constant, and  $\gamma = 6$  is the parameter in the definition of the Gaussian filter.

The computational domain is periodic in the streamwise ( $x$ ) and spanwise ( $z$ ) directions, and the pressure gradient that drives the flow is adjusted dynamically to maintain a constant mass flux through the channel. The parameters used in the numerical simulations are given in Table 1 for the two Reynolds numbers considered ( $Re_\tau = 180$  and  $Re_\tau = 395$ ). The filter width  $\delta$  is computed as  $\delta = \sqrt[3]{\Delta_x \Delta_z \Delta_y(y)}$ , where  $\Delta_x$  and  $\Delta_z$  are the largest spaces between the Gauss-Lobatto-Legendre (GLL) points in the  $x$  and  $z$  directions, respectively, and  $\Delta_y(y)$  is inhomogeneous and is computed as an interpolation function that is zero at the wall and is twice the normal mesh size for the elements in the center of the channel.

The numerical simulations were performed by using a spectral element code based on the  $\mathbb{P}_N - \mathbb{P}_{N-2}$  velocity and pressure spaces introduced by Maday and Patera [44]. The domain is decomposed into spectral elements, as shown in Figure 3. Mesh spacing in the wall-normal direction ( $y$ ) was chosen to be roughly equivalent to a Chebychev distribution having the same number of points. The velocity is continuous across element interfaces and

is represented by  $N$ th-order tensor-product Lagrange polynomials based on the GLL points. The pressure is discontinuous and is represented by tensor-product polynomials of degree  $N - 2$ . Time stepping is based on an operator-splitting of the discrete system, which leads to separate convective, viscous, and pressure subproblems without the need for ad hoc pressure boundary conditions. A filter, which removes 2%–5% of the highest velocity mode, is used to stabilize the Galerkin formulation [45]; the filter does not compromise the spectral accuracy. Details of the discretization and solution algorithm are given in [46], [47].

The initial conditions for the  $Re_\tau = 180$  simulations were obtained by superimposing a 2D Tollmien-Schlichting (TS) mode of 2% amplitude and a 3D TS mode of 1% amplitude on a parabolic mean flow (Poiseuille flow) and integrating the flow for a long time (approximately  $200 H/u_\tau$ , where  $H$  is the channel’s halfwidth and  $u_\tau$  is the wall shear velocity) on a finer mesh ( $72 \times 73 \times 72$  mesh points). The final field file was further integrated on the actual coarse LES mesh ( $36 \times 37 \times 36$  mesh points) for approximately  $50 H/u_\tau$  to obtain the initial condition for *all* four  $Re_\tau = 180$  simulations.

The initial condition for the  $Re_\tau = 395$  case was obtained in a similar manner: We started with a field file corresponding to a  $Re_\tau = 180$  simulation, and we integrated it on a finer mesh ( $96 \times 73 \times 72$  mesh points) for a long time (approximately  $50 H/u_\tau$ ). Then, we integrated the resulting flow on the actual coarser LES mesh ( $72 \times 55 \times 54$  mesh points) for another  $40 H/u_\tau$ , and the final field file was used as initial condition for *all* four simulations.

For each of the four simulations and for both  $Re_\tau = 180$  and  $Re_\tau = 395$ , the flow was integrated further in time until the statistically steady state was reached (for approximately  $15 H/u_\tau$ ). The statistically steady state was identified by a linear total shear stress profile (see Figure 4 and Figure 5).

The statistics were then collected over another  $5 H/u_\tau$  and contained samples taken after each time step ( $\Delta t = 0.0002$  for  $Re_\tau = 180$  and  $\Delta t = 0.00025$  for  $Re_\tau = 395$ ). We also averaged over the two halves of the channel.

In our numerical experiments, we considered, as a first step, homogeneous boundary conditions for all LES models tested.

The numerical results include plots of the following time- and plane-averaged quantities normalized by the *computed*  $u_\tau$ : the mean streamwise velocity  $\ll \bar{u} \gg / u_\tau$ ; the  $x, y$ -component of the Reynolds stress  $\ll u'v' \gg / u_\tau^2$ ; and the rms values of the streamwise  $\ll u'u' \gg / u_\tau^2$ ; wall-normal  $\ll v'v' \gg / u_\tau^2$ , and spanwise  $\ll w'w' \gg / u_\tau^2$  velocity fluctuations, where  $\ll \cdot \gg$  denotes time and plane ( $xz$ ) averaging, the fluctuating quantities  $f'$  are calculated as  $f' = f - \ll f \gg$ , and a “+” superscript denotes the variable in wall units.

Note that in our simulations the bulk velocity  $U_m$  was fixed to match the corresponding one in [43] (see Table 2), and the friction velocity  $u_\tau$  was a result of the simulations. Table 2 presents the *actual* values of  $Re_\tau$  corresponding to the friction velocity  $u_\tau$  computed for all four numerical tests and two nominal Reynolds numbers. We note that the friction velocity  $u_\tau$  is within 1%–2% of the nominal value, and, as a result, so is the actual  $Re_\tau$ .

## 4 *A Posteriori* Tests for $Re_\tau = 180$

We ran *a posteriori* tests for the RLES model (12), the gradient model (9), the Smagorinsky model, and a coarse DNS (no model). We compared the corresponding results with the fine DNS simulation of Moser, Kim, and Mansour [43].

Figure 6 shows the normalized mean streamwise velocity; note the almost perfect overlapping of the results corresponding to the models tested. We interpret this behavior as a measure of our success in enforcing a constant mass flux through the channel.

Figure 7 presents the normalized  $x, y$ -component of the Reynolds stress. The RLES model (12) is a clear improvement over the rest (i.e., closest to the fine DNS).

Similarly, the normalized rms values of the streamwise velocity fluctuations in Figure 8 show a better (closer to the fine DNS benchmark results in [43]) behavior for the RLES model (12).

Figures 9 and 10, containing the normalized rms values for the wall-normal and spanwise velocity fluctuations, merit a more detailed discussion. Figure 9 shows the normalized rms values of the wall-normal velocity fluctuations. Here, the RLES model (12) performs worse than the gradient model (9) near the wall. Away from the wall, the gradient and the RLES model perform similarly. The best results are obtained with the Smagorinsky model.

The normalized rms values of the spanwise velocity fluctuations in Figure 10 are better for the RLES model (12) than for the gradient model, except for a portion of  $1 - |y|$  roughly between 0.3 and 0.5. The Smagorinsky model gives the best results near the wall, but it overpredicts the correct value near the center of the channel.

In conclusion, the RLES model (12) performs better than the gradient model, with the exception of the normalized rms values of the wall-normal velocity fluctuations. The RLES model (12) is also more stable numerically than the gradient model.

## 5 *A Posteriori* Tests for $Re_\tau = 395$

We ran simulations with all four models for  $Re_\tau = 395$ , and we compared our results with the fine DNS in [43]. Again, as in the  $Re_\tau = 180$  case, the normalized mean streamwise velocity fluctuations in Figure 11 are practically identical; this time, however, they do not overlap onto that corresponding to the fine DNS. Nevertheless, the mean flows are the same, and this is supported by the fact that the models underpredict the correct value near the wall but overpredict it away from the wall.

The normalized  $x, y$ -component of the Reynolds stress in Figure 12 is almost identical for all four models. This behavior was also noticed by Winckelmans et al. [23].

The same behavior can be noticed for the normalized rms values of the streamwise velocity fluctuations in Figure 13: the profiles for the four models are almost identical. The RLES model (12) performs slightly better near the wall, and the gradient model performs slightly



better away from the wall. They both perform better than the Smagorinsky model near the center of the channel.

Figure 14 presents the normalized rms values of the wall-normal velocity fluctuations. As for the  $Re_\tau = 180$  case, the gradient model performs better near the wall, and the RLES model (12) performs better away from the wall. The Smagorinsky model performs best, but it overpredicts the correct value near the center of the channel.

The same behavior is observed for the normalized rms values of the spanwise velocity fluctuations in Figure 15, and again the Smagorinsky model performs best.

In conclusion, for the  $Re_\tau = 395$  case, the gradient and the RLES model (12) yield comparable results. The best results, however, are obtained by using the Smagorinsky model.

Again, as in the  $Re_\tau = 180$  case, the RLES model (12) is much more stable numerically than the gradient model.

## 6 Conclusions

We have used a spectral element code to test the RLES model (12) in the numerical simulation of incompressible channel flows at  $Re_\tau = 180$  and  $Re_\tau = 395$ . This approximate deconvolution model is based on a rational (Padé) approximation to the Fourier transform of the Gaussian filter and is proposed as an alternative to the gradient model (9). We compared the RLES model (12) with the gradient model, the Smagorinsky model, and a coarse DNS (no LES model). The corresponding results were benchmarked against the fine DNS calculation of Moser, Kim, and Mansour [43].

The RLES model (12) yielded the best results for the  $Re_\tau = 180$  case. These improved results were accompanied by a much increased numerical stability compared with the gradient model.

The situation was different for the  $Re_\tau = 395$  case. Here the RLES model (12) and the gradient model yielded comparable results, and the Smagorinsky model performed the best. Again, the RLES model (12) was much more stable numerically than the gradient model.

We believe that these results for the RLES model are encouraging. They also support our initial thoughts: The RLES model is an improvement over the gradient model as a subfilter-scale model, and this is illustrated by the improved results for the  $Re_\tau = 180$  case. The RLES model is also more stable numerically because of the additional smoothing operator, and this feature is manifest for both low ( $Re_\tau = 180$ ) and moderate ( $Re_\tau = 395$ ) Reynolds number flows.

However, the RLES model accounts just for the subfilter-scale part of the stress reconstruction. The information lost at the subgrid-scale level must be accounted for in a different way, as advocated by Carati et al. [24]. This was illustrated by the fact that, even for a moderate Reynolds number ( $Re_\tau = 395$ ) flow, the Smagorinsky model, a classical eddy-viscosity

model, performed best.

Along these lines, our next step will be to develop a mixed model, consisting of the RLES model supplemented by a Smagorinsky model. We also plan to study improved boundary conditions, the commutation error [48], [49], and the relationship between the filter radius and the mesh-size in a spectral element discretization.

**Acknowledgments.** This work was supported in part by the Mathematical, Information, and Computational Sciences Division subprogram of the Office of Advanced Scientific Computing Research, U.S. Dept. of Energy, under Contract W-31-109-Eng-38.

We thank Professor R. Moser and Mr. A. Das for helpful communications that improved this paper.

## References

- [1] C. Meneveau and J. Katz, “Scale invariance and turbulence models for large-eddy simulation,” *Annu. Rev. Fluid Mech.* **32**, 1 (2000).
- [2] M. Lesieur and O. Métais, “New trends in large-eddy simulations of turbulence,” *Annu. Rev. Fluid Mech.* **28**, 45 (1996).
- [3] P. Sagaut, *Large Eddy Simulation for Incompressible Flows* (Springer Verlag, Berlin, 2001).
- [4] J. Smagorinsky, “General circulation experiments with the primitive equation: I the basic experiment,” *Mon. Wea. Rev.* **91**, 99 (1963).
- [5] R. A. Clark, J. H. Ferziger, and W. C. Reynolds, “Evaluation of subgrid scale models using an accurately simulated turbulent flow,” *J. Fluid Mech.* **91**, 1 (1979).
- [6] J. Bardina, J. H. Ferziger, and W. C. Reynolds, “Improved turbulence models based on large eddy simulation of homogeneous, incompressible, turbulent flows,” Technical Report No. TF-19, Department of Mechanical Engineering, Stanford University, Stanford, CA, 1983.
- [7] M. Germano, U. Piomelli, P. Moin, and W. Cabot, “A dynamic subgrid-scale eddy viscosity model,” *Phys. Fluids A* **3**, 1760 (1991).
- [8] U. Piomelli, “High Reynolds number calculations using the dynamic subgrid-scale stress model,” *Phys. Fluids A* **5**, 1484 (1993).
- [9] K. Horiuti, “A new dynamic two-parameter mixed model for large-eddy simulation,” *Phys. Fluids* **9**, 3443 (1997).
- [10] F. Sarghini, U. Piomelli, and E. Balaras, “Scale-similar models for large-eddy simulations,” *Phys. Fluids* **11**, 1596 (1999).
- [11] K. B. Shah and J. Ferziger, “A new non-eddy viscosity subgrid-scale model and its application to turbulent flow,” in *CTR Annual Research Briefs 1995*, Center for Turbulence Research, Stanford University and NASA Ames Research Center, Stanford, CA, 1995.
- [12] B. J. Geurts, “Inverse modeling for large-eddy simulation,” *Phys. Fluids* **9**, 3585 (1997).
- [13] G. J. M. Kuerten, B. J. Geurts, A. W. Vreman, and M. Germano, “Dynamic inverse-modeling and its testing in large-eddy simulation of the mixing layer”, *Phys. Fluids* **11**, 3778 (1999).

- [14] J. A. Domaradzki and E. M. Saiki, "A subgrid-scale model based on the estimation of unresolved scales of turbulence," *Phys. Fluids* **9**, 2148 (1997).
- [15] J. A. Domaradzki and K.-C. Loh, "The subgrid-scale estimation model in physical space estimation," *Phys. Fluids* **11**, 2330 (1999).
- [16] K.-C. Loh and J. A. Domaradzki, "The subgrid-scale estimation model on nonuniform grids," *Phys. Fluids* **11**, 3786 (1999).
- [17] S. Stolz and N. A. Adams, "An approximate deconvolution procedure for large-eddy simulation," *Phys. Fluids* **11**, 1699 (1999).
- [18] S. Stolz, N. A. Adams, and L. Kleiser, "An approximate deconvolution model for large-eddy simulation with application to incompressible wall-bounded flows," *Phys. Fluids* **13**, 997 (2001).
- [19] S. Stolz, N. A. Adams, and L. Kleiser, "The approximate deconvolution model for large-eddy simulations of compressible flows and its application to shock-turbulent-boundary-layer interaction," *Phys. Fluids* **13**, 2985 (2001).
- [20] A. Leonard, "Energy cascade in large eddy simulations of turbulent fluid flows," *Adv. in Geophysics* **18A**, 237 (1974).
- [21] S. Liu, C. Meneveau, and J. Katz, "On the properties of similarity subgrid-scale models as deduced from measurements in a turbulent jet," *J. Fluid Mech.* **275**, 83 (1994).
- [22] V. Borue and S.A. Orszag, "Local energy flux and subgrid-scale statistics in three-dimensional turbulence," *J. Fluid Mech.* **366**, 1 (1998).
- [23] G. S. Winckelmans, A. A. Wray, O. V. Vasilyev, and H. Jeanmart, "Explicit-filtering large-eddy simulations using the tensor-diffusivity model supplemented by a dynamic Smagorinsky term," *Phys. Fluids* **13**, 1385 (2001).
- [24] D. Carati, G. S. Winckelmans, and H. Jeanmart, "On the modeling of the subgrid-scale and filtered-scale stress tensors in large-eddy simulation," *J. Fluid Mech.* **441**, 119 (2001).
- [25] B. Vreman, "Direct and large-eddy simulation of the compressible turbulent mixing layer", Ph.D. thesis, University of Twente, 1995.
- [26] G.-H. Cottet and A. A. Wray, "Anisotropic grid-based formulas for subgrid-scale models," in *Annual Research Briefs, Center for Turbulence Research, Stanford University and NASA Ames*, 1997, pp. 113–122.

- [27] G.-H. Cottet and O. V. Vasilyev, “Comparison of dynamic Smagorinsky and anisotropic subgrid-scale models,” Proceedings of the Summer Program, Center for Turbulence Research, Stanford University and NASA Ames, 1998, pp. 367–388.
- [28] B. Vreman, B. Geurts, and H. Kuerten, “Large-eddy simulation of the temporal mixing layer,” *J. Fluid Mech.* **339**, 357 (1997).
- [29] G. P. Galdi and W. J. Layton, “Approximating the larger eddies in fluid motion II: a model for space filtered flow,” *Math. Models and Methods in App. Sci.* **10**, 343 (2000).
- [30] B. Vreman, B. Geurts, and H. Kuerten, “Large-eddy simulation of the temporal mixing layer using the mixed Clark model,” *Theor. Comput. Fluid Dyn.* **8**, 309 (1996).
- [31] A. A. Aldama, *Filtering Techniques for Turbulent Flow Simulation*, edited by C. A. Brebbia and S. A. Orszag (Lecture Notes in Engineering **56**, Springer-Verlag, 1990).
- [32] F. V. Katopodes, R. L. Street, and J.H. Ferziger, “Subfilter-scale scalar transport for large-eddy simulation,” in *14th Symposium on Boundary Layer and Turbulence*, (American Meteorological Society, 2000), pp. 472–475.
- [33] M. Germano, “Differential filters for the large eddy numerical simulation of turbulent flows,” *Phys. Fluids* **29**, 1755 (1986).
- [34] J. S. Mullen and P. F. Fischer, “Filtering techniques for complex geometry fluid flows,” *Commun. Numer. Meth. Engng.* **15**, 9 (1999).
- [35] J. A. Domaradzki and D. D. Holm, “Navier-Stokes-alpha model: LES equations with nonlinear dispersion,” in *Modern Simulation Strategies for Turbulent Flow*, edited by B. J. Geurts, (ERCOFTAC Bulletin **48**, 2001).
- [36] L. C. Berselli, G. P. Galdi, T. Iliescu, and W. J. Layton, “Mathematical analysis for the rational large eddy simulation model,” *Math. Models and Methods in App. Sci.*, accepted (2002).
- [37] P. Coletti, “A global existence theorem for large eddy simulation turbulence model,” *Math. Models and Methods in App. Sci.* **7**, 579 (1997).
- [38] T. Iliescu, V. John, and W. J. Layton, “Convergence of finite element approximation of large eddy motion,” *Num. Meth. Part. Diff. Eq.*, accepted pending revisions (2002).
- [39] T. Iliescu, V. John, W. J. Layton, G. Matthies, and L. Tobiska, “A numerical study of a class of LES models,” submitted (2002).

- [40] P. Fischer and T. Iliescu, “A 3D channel flow simulation at  $Re_\tau = 180$  using a rational LES model,” in *Proceedings of Third AFOSR International Conference on DNS/LES*, edited by C. Liu, L. Sakell, and T. Beutner, (Greyden Press, Columbus, 2001) pp. 283–290.
- [41] P. Moin and J. Kim, “Numerical investigation of turbulent channel flow,” *J. Fluid Mech.* **118**, 341 (1982).
- [42] J. Kim, P. Moin, and R. Moser, “Turbulence statistics in fully developed channel flow at low Reynolds number,” *J. Fluid Mech.* **177**, 133 (1987).
- [43] D. R. Moser, J. Kim, and N. N. Mansour, “Direct numerical simulation of turbulent channel flow up to  $Re_\tau = 590$ ,” *Phys. Fluids* **11**, 943 (1999).
- [44] Y. Maday and A. T. Patera, “Spectral element methods for the Navier-Stokes equations,” in *State of the Art Surveys in Computational Mechanics*, edited by A. K. Noor (ASME, New York, 1989) pp. 71–143.
- [45] P. F. Fischer and J. S. Mullen, “Filter-based stabilization of spectral element methods,” *Comptes rendus de l’Académie des sciences Paris*, t. 332, -Série I - Analyse numérique, 265 (2001).
- [46] P. F. Fischer, “An overlapping Schwarz method for spectral element solution of the incompressible Navier-Stokes equations,” *J. Comp. Phys.* **133**, 84 (1997).
- [47] P. F. Fischer, N. I. Miller, and H. M. Tufo, “An overlapping Schwarz method for spectral element simulation of three-dimensional incompressible flows,” in *Parallel Solution of Partial Differential Equations*, edited by P. Björstad and M. Luskin (Springer-Verlag, 2000), pp. 159-181.
- [48] S. Ghosal and P. Moin, “The basic equations for the large-eddy simulation of turbulent flows in complex geometry,” *J. Comput. Phys.* **118**, 24 (1995).
- [49] S. Ghosal, “An analysis of numerical errors in large-eddy simulations of turbulence,” *J. Comput. Phys.* **125**, 187 (1996).

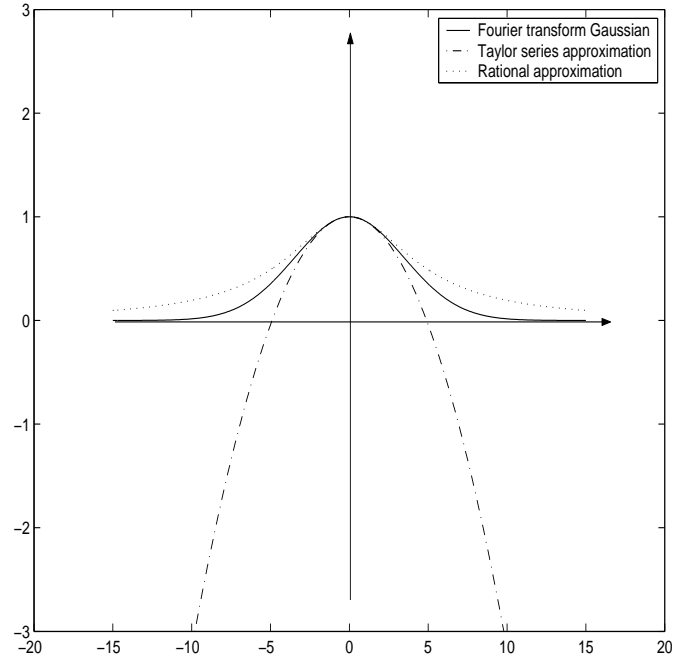


Figure 1: Approximations to the Fourier transform of the Gaussian filter: Rational (Padé) vs. Taylor.

Table 1: Parameters for the numerical simulations.

Nominal $Re_\tau$	$L_x \times L_y \times L_z$	$N_x \times N_y \times N_z$
180	$4\pi \times 2 \times \frac{4}{3}\pi$	$36 \times 37 \times 36$
395	$2\pi \times 2 \times \pi$	$72 \times 55 \times 54$



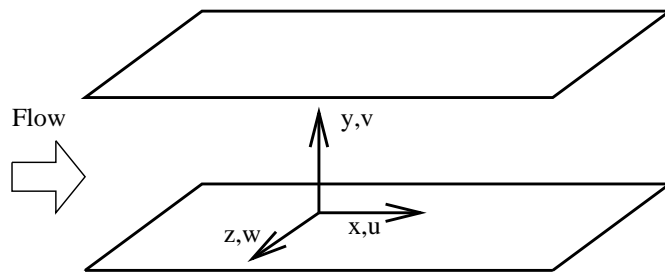


Figure 2: Problem setup for the channel flow.

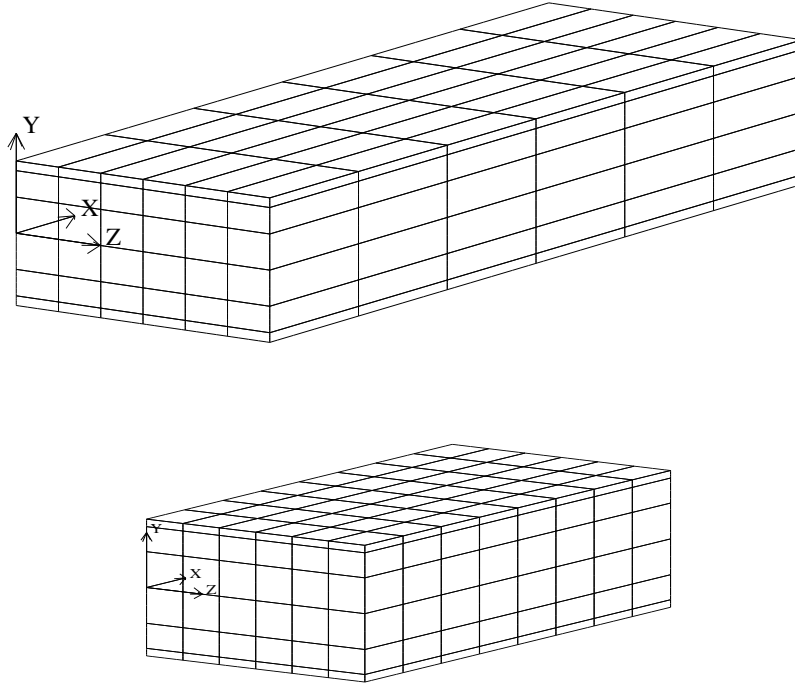


Figure 3: Spectral element meshes:  $Re_\tau = 180$  (top), and  $Re_\tau = 395$  (bottom).

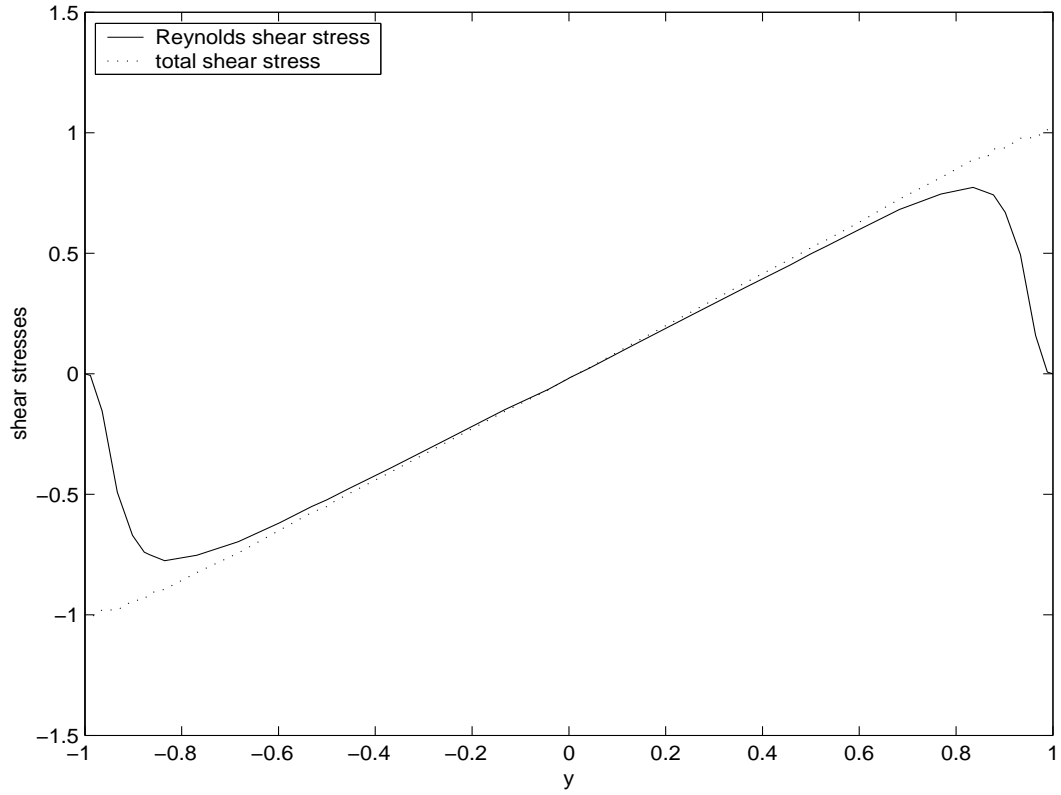


Figure 4:  $Re_\tau = 180$ , linear total shear stress profile, an indication that the statistically steady state was reached.

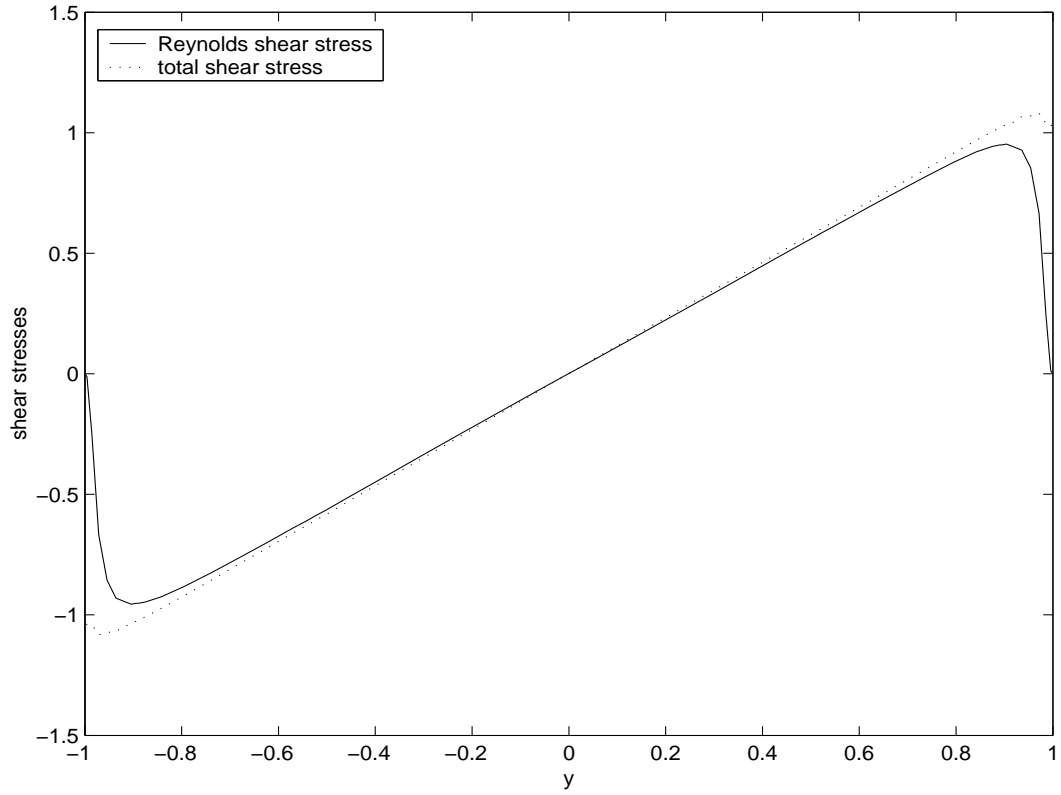


Figure 5:  $Re_\tau = 395$ , linear total shear stress profile, an indication that the statistically steady state was reached.

Table 2: Computed  $u_\tau$  and  $Re_\tau$ .

Fixed $U_m$	Nominal $Re_\tau$	Case	Computed $u_\tau$	Computed $Re_\tau$
15.63	180	RLES	0.9879448	177.8352
		gradient	0.9890118	178.0222
		Smagorinsky	0.9917144	178.5120
		coarse DNS	0.9873800	177.7184
17.54	395	RLES	1.001025319	395.4071960
		gradient	1.005021334	396.9859924
		Smagorinsky	0.9974176884	393.9718933
		coarse DNS	0.9901855588	391.1294861

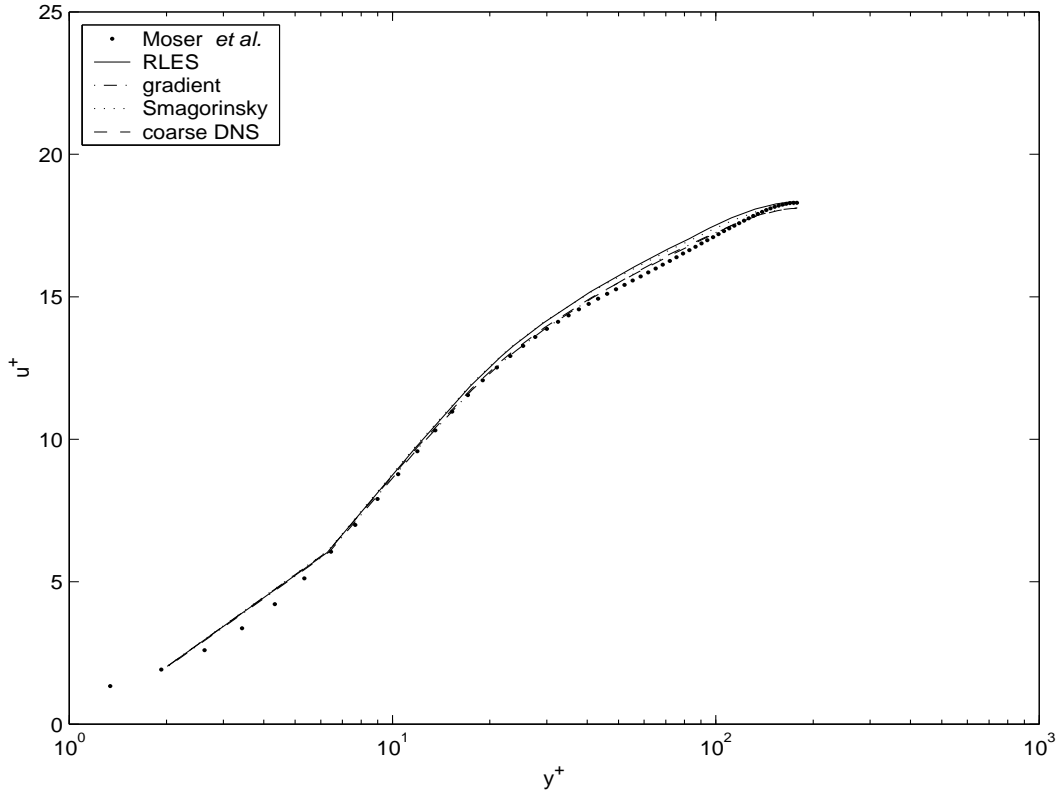


Figure 6: Mean streamwise velocity,  $Re_\tau = 180$ . We compared the RLES model (12), the gradient model (9), the Smagorinsky model, and a coarse DNS, with the fine DNS of Moser, Kim, and Mansour [43].

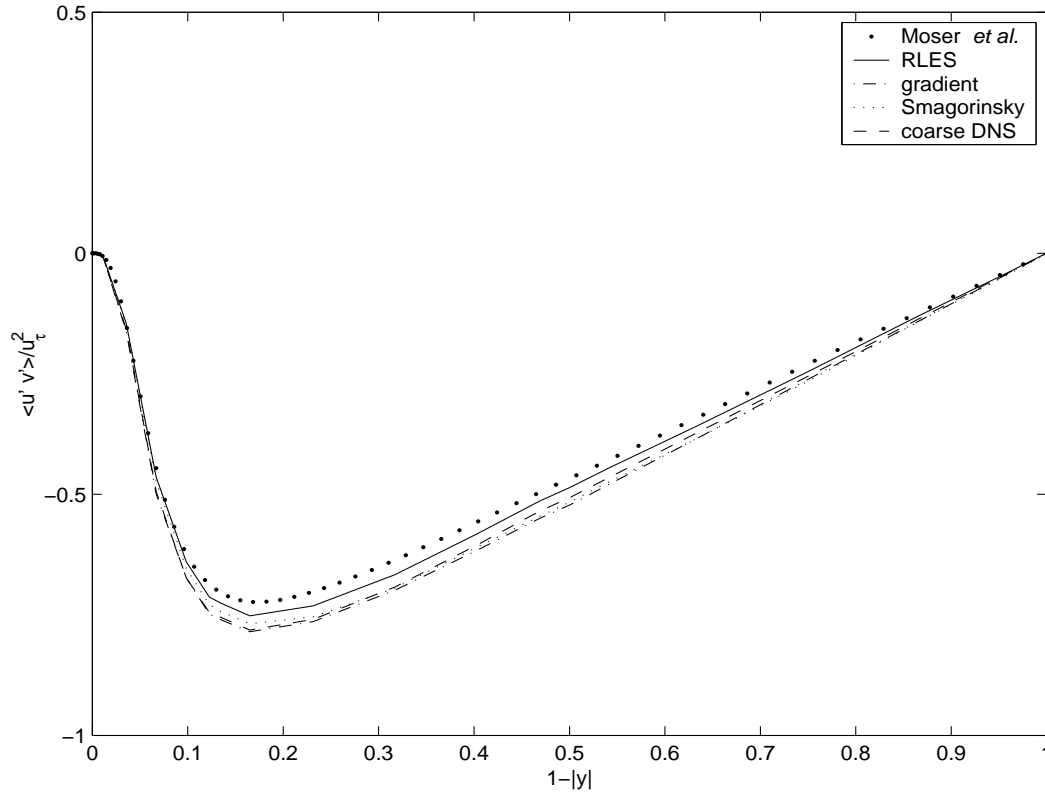


Figure 7: The  $x, y$ -component of the Reynolds stress,  $Re_\tau = 180$ . We compared the RLES model (12), the gradient model (9), the Smagorinsky model, and a coarse DNS, with the fine DNS of Moser, Kim, and Mansour [43].

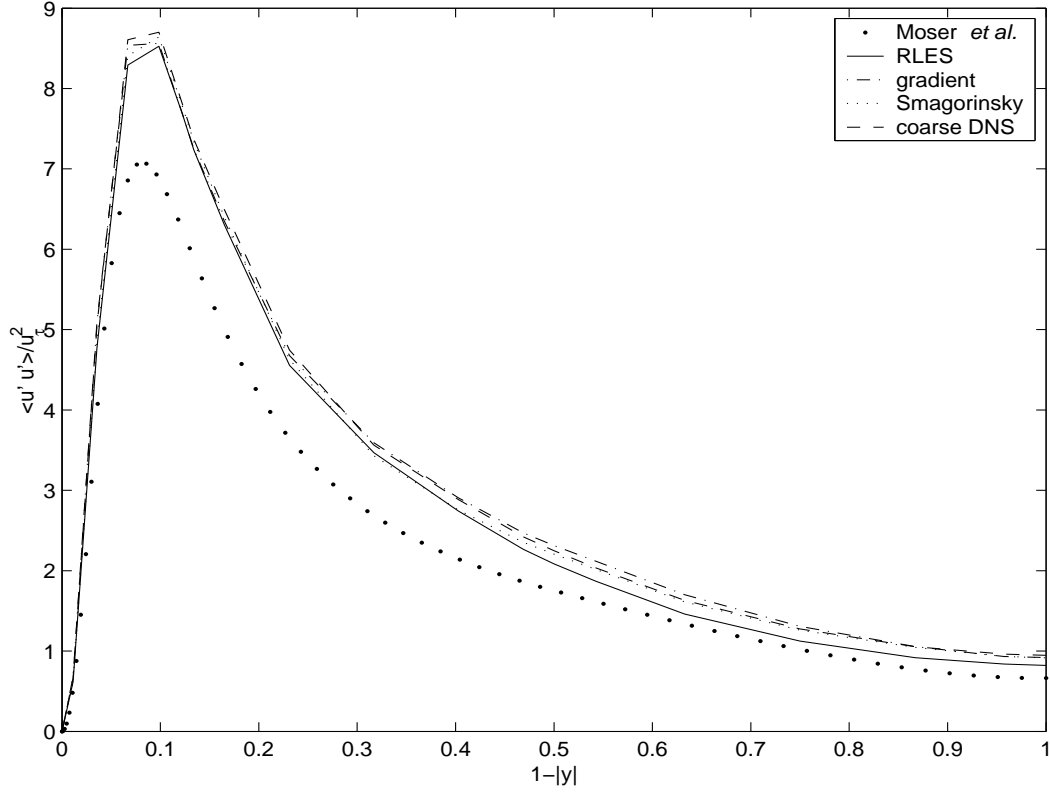


Figure 8: Rms values of streamwise velocity fluctuations,  $Re_\tau = 180$ . We compared the RLES model (12), the gradient model (9), the Smagorinsky model, and a coarse DNS, with the fine DNS of Moser, Kim, and Mansour [43].



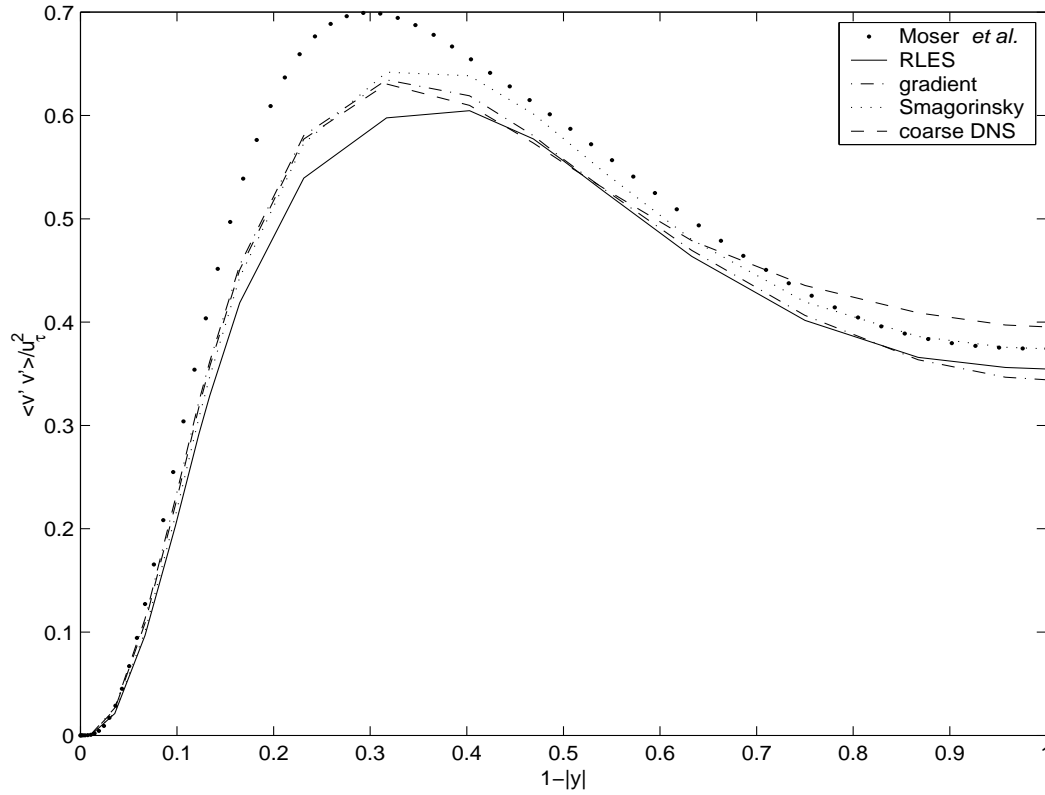


Figure 9: Rms values of wall-normal velocity fluctuations,  $Re_\tau = 180$ . We compared the RLES model (12), the gradient model (9), the Smagorinsky model, and a coarse DNS, with the fine DNS of Moser, Kim, and Mansour [43].

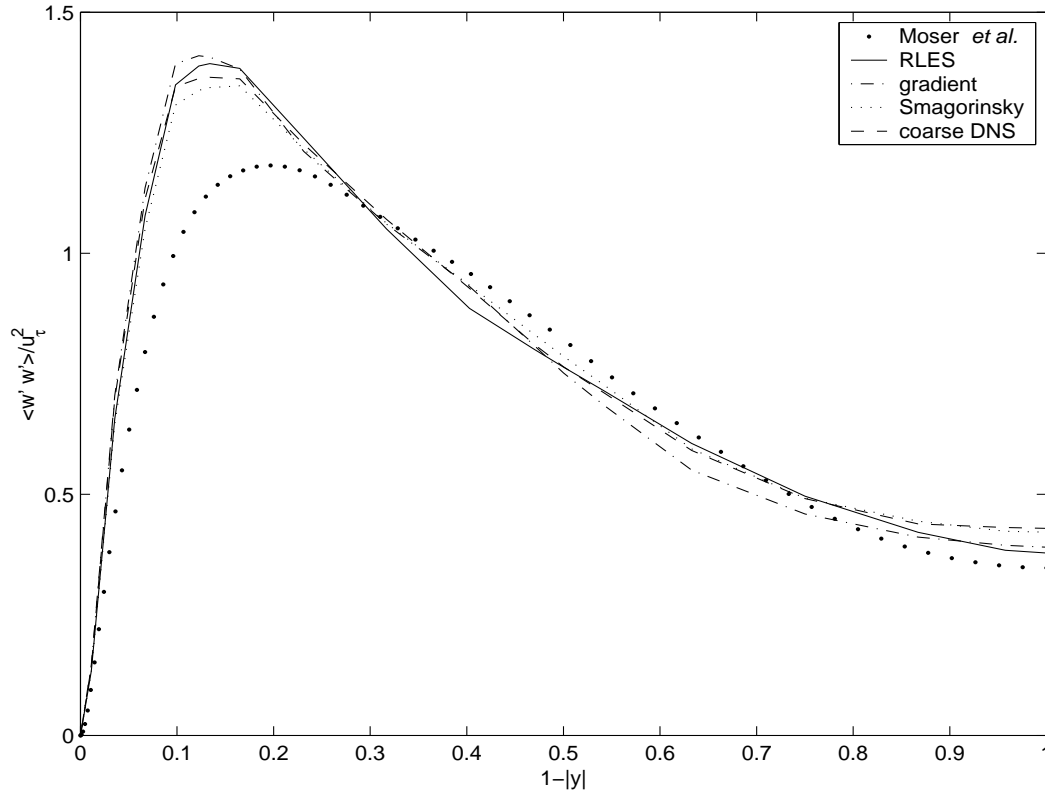


Figure 10: Rms values of spanwise velocity fluctuations,  $Re_\tau = 180$ . We compared the RLES model (12), the gradient model (9), the Smagorinsky model, and a coarse DNS, with the fine DNS of Moser, Kim, and Mansour [43].

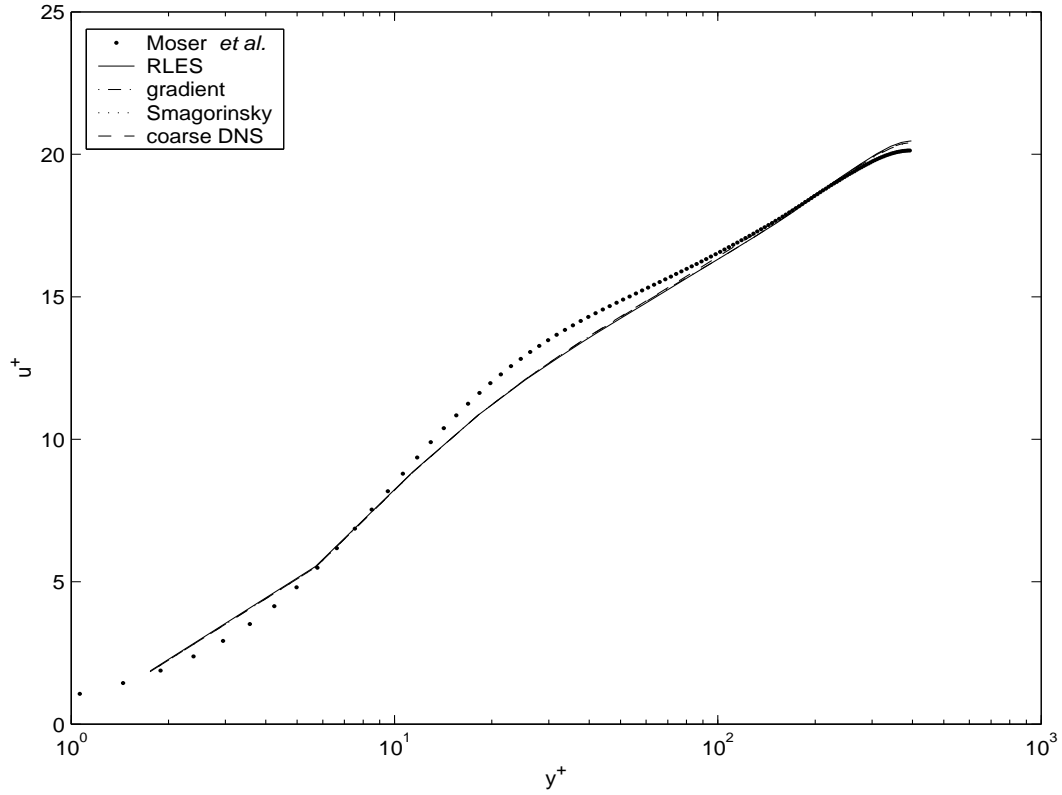


Figure 11: Mean streamwise velocity,  $Re_\tau = 395$ . We compared the RLES model (12), the gradient model (9), the Smagorinsky model, and a coarse DNS, with the fine DNS of Moser, Kim, and Mansour [43].

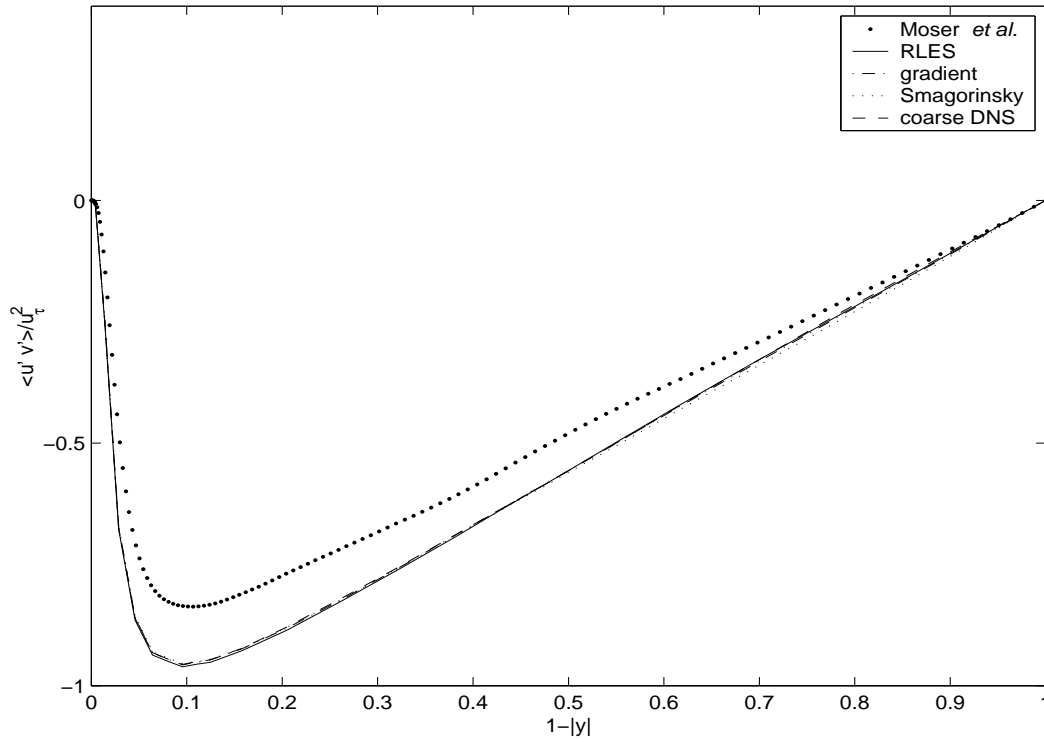


Figure 12: The  $x, y$ -component of the Reynolds stress,  $Re_\tau = 395$ . We compared the RLES model (12), the gradient model (9), the Smagorinsky model, and a coarse DNS, with the fine DNS of Moser, Kim, and Mansour [43].

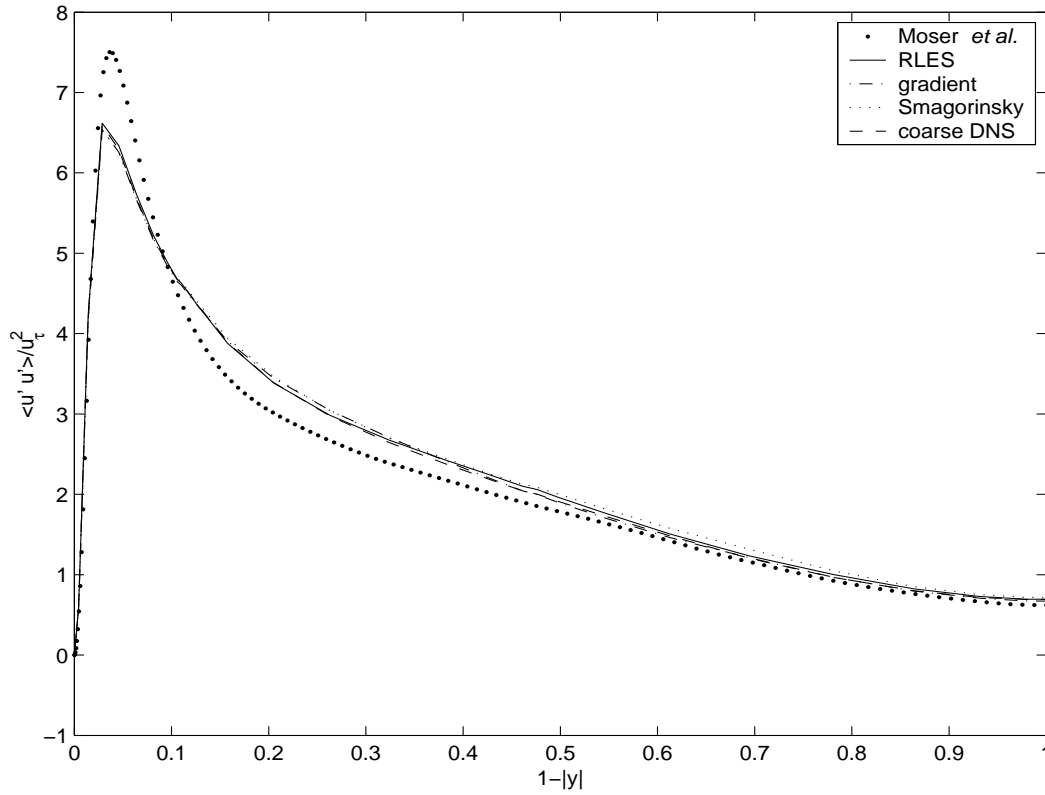


Figure 13: Rms values of streamwise velocity fluctuations,  $Re_\tau = 395$ . We compared the RLES model (12), the gradient model (9), the Smagorinsky model, and a coarse DNS, with the fine DNS of Moser, Kim, and Mansour [43].

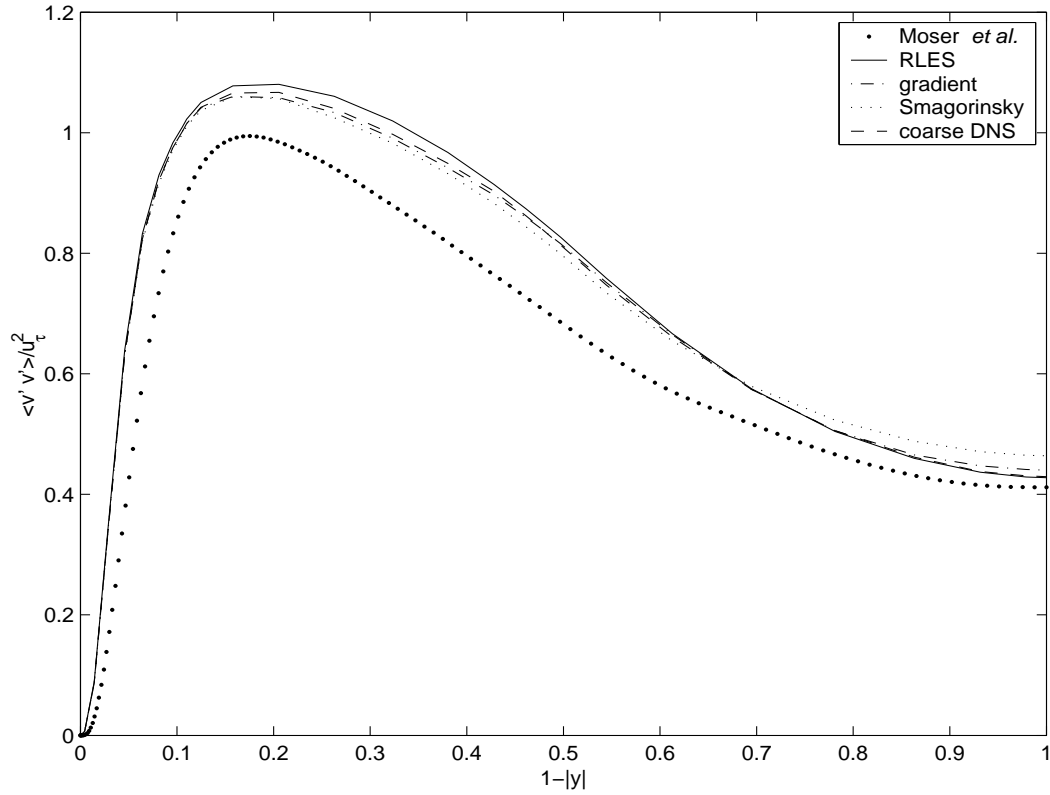


Figure 14: Rms values of wall-normal velocity fluctuations,  $Re_\tau = 395$ . We compared the RLES model (12), the gradient model (9), the Smagorinsky model, and a coarse DNS, with the fine DNS of Moser, Kim, and Mansour [43].

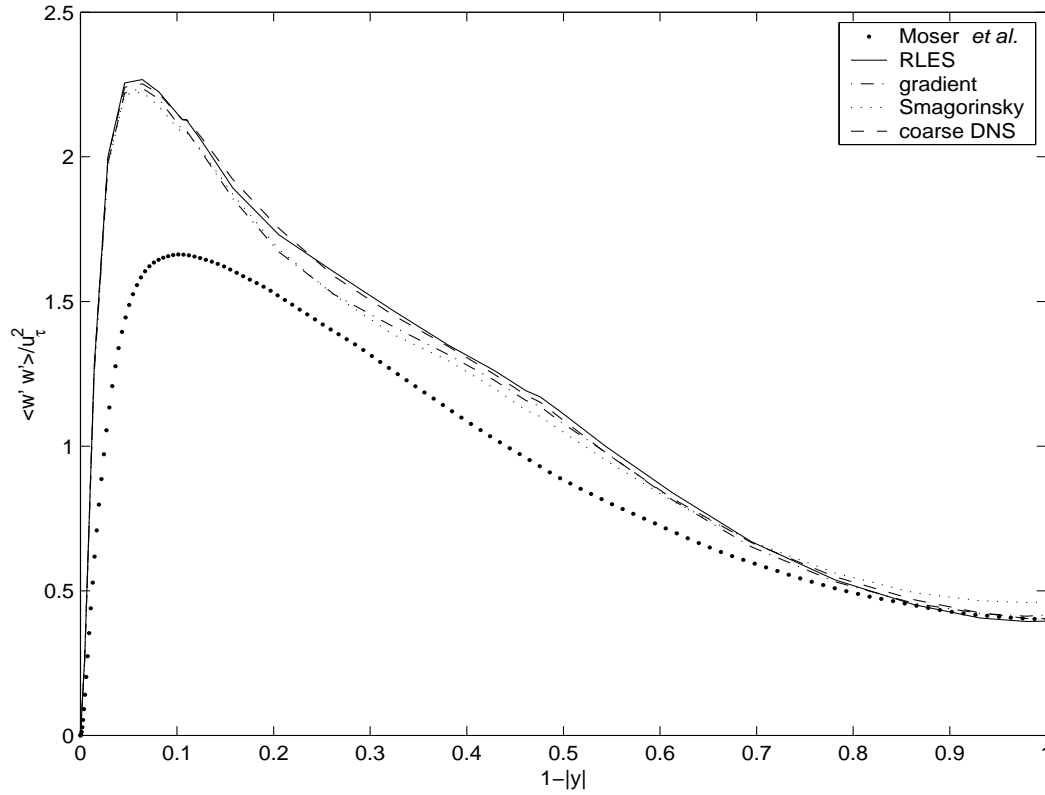


Figure 15: Rms values of spanwise velocity fluctuations,  $Re_\tau = 395$ . We compared the RLES model (12), the gradient model (9), the Smagorinsky model, and a coarse DNS, with the fine DNS of Moser, Kim, and Mansour [43].

